Effect of warm accumulative roll bonding on the evolution of microstructure, texture and creep properties in the 7075 aluminium alloy

(Mater Sci Eng A 556 (2012) 287-294 DOI 10.1016/j.msea.2012.06.089)

P. Hidalgo-Manrique*, C.M. Cepeda-Jiménez, O.A. Ruano, F. Carreño

Department of Physical Metallurgy, CENIM-CSIC, Av. Gregorio del Amo 8, 28040 Madrid, Spain.

**Corresponding autor: Tel.: +34 91 5538900; Fax: +34 91 5347425; E-mail address: hidalgo@cenim.csic.es*

Abstract

The commercial 7075 Al alloy was severely deformed at 300ºC by a 3:1 thickness reduction per pass accumulative roll bonding (ARB) process up to 5 passes. Examinations by transmission electron microscopy and electron backscatter diffraction revealed that the alloy microstructure was finer and more misoriented with increasing the number of ARB passes. The 5-passes sample exhibited a mean cell/(sub)grain diameter of 355 nm and a mean boundary misorientation angle of 33º. The texture of the processed alloy was characterized by a β-fibre, whose intensity increased with increasing the number of ARB passes. This intensification process is enhanced by the cutting and stacking steps promoting the formation of the Dillamore orientation. Uniaxial tensile tests conducted at 300ºC and at an initial strain rate of 10^{-2} s^{-1} revealed that the processed alloy exhibited superplasticity, which was very sensitive to the stability of its microstructure at the testing temperature. An elongation to failure of 202% was registered for the 4-passes sample. Therefore, the present ARB process would allow short forming times at much lower temperatures than conventional.

Keywords: accumulative roll bonding; 7075 aluminium alloy; grain refinement; rolling texture; superplasticity.

1. Introduction

The materials used for aeronautical applications must mainly fulfil the following conditions: low weight, high availability, good formability, low cost, high reliability and easy maintainability. This is the reason why the aluminium alloys have been the primary material of choice for structural components of aircrafts since the beginning of the 20th century. One of the most popular aluminium alloys in the aeronautical industry is the 7075 Al alloy which, due to its excellent strength/weight ratio, is widely used for the fuselage, the wings and the supporting structure [1].

Grain boundary sliding (GBS) is a diffusion-controlled creep mechanism which occurs at low stress by the movement of individual grains sliding past one another along their common boundary. The most important phenomenon that may result from GBS is an enhanced ductility or superplasticity [2]. Superplasticity is an important field of scientific research because it forms the underlying basis for superplastic forming (SPF). SPF is a well-established industrial process for the fabrication of complex shapes in sheet metals, which is especially used by the aircraft industry [3].

It is well established that two basic requirements must be fulfilled in order to achieve superplastic flow [4]. First, superplasticity requires equiaxed, misoriented and fine (typically < 10 μm) grains, which can be obtained by adequate processing. Second, superplasticity is a diffusion-controlled process and, therefore, it requires a relatively high temperature (typically at or above $\sim 0.5\ T_m$, where T_m is the absolute melting temperature of the material). Additionally, for a given superplastic material and at a given temperature, there is a maximum strain rate where superplastic flow by GBS is no longer the dominant process; another

deformation mechanism becomes controlling, namely diffusion-controlled dislocation creep [5]. The maximum strain rate at which grain boundary remains rate controlling is typically of the order of 10^{-4} s^{-1}, which restricts the commercial applications of SPF to a limited range of low-volume high-value components [3]. However, a number of experimental investigations [6,7] reveal that it is possible to increase the maximum strain rate for superplastic flow by making a substantial reduction in the grain size.

Severe plastic deformation (SPD) is an effective method of producing ultra-fine grained (UFGed) materials (mean grain diameter < 1 μm). Various SPD processes such as equal channel angular pressing (ECAP) [8], high pressure torsion (HPT) [9] and accumulative roll bonding (ARB) [10] have been developed. They all allow the production of UFGed bulk materials in a relatively simple and inexpensive way. Additionally, these processes lead to materials free of pores and impurities.

Among such processes, ARB is the most appropriate for practical applications because it can be readily carried out by conventional rolling equipments and it is the only one appropriate to manufacture sheets or plates, the most widely used material shape in the industrial field [11], including the SPF industry. The ARB process has been widely and successfully performed on pure aluminium [12] and different aluminium alloys, such as AA6061 [13], AA3003 [14], AA8006 [15], AA5086 [16] and A356 [17]. However, low attention has been paid to the 7075 aluminium alloy [18,19], despite its very high aeronautical significance.

In the present investigation, a commercial 7075 Al alloy was severely processed by ARB. The ARB process was conducted at 300ºC applying thickness reductions of 3:1. The work was conducted to evaluate the potential of the present ARB process to achieve fine and highly misoriented microstructures and superplasticity at a temperature as low as 300ºC and at

a strain rate as high as 10^{-2} s^{-1}. Additionally, the evolution of the microstructure, texture and mechanical properties with the number of ARB passes (N) were carefully examined.

2. Material and experimental procedure

The material used for the present work was the commercial 7075 Al alloy, provided in the T6 condition. The chemical composition is shown in Table 1. From the as-received alloy sheet two pieces with dimensions 2 mm × 30 mm × 180 mm were cut, cleaned with methyl ethyl ketone, put one on top of the other and fastened by steel wires. The resulting 4 mm-thick specimen was held for 5 minutes at 300ºC in a preheated electric furnace and, straight afterwards, undergone a thickness reduction of 3:1, equivalent to a true strain of 1.1, by a single rolling pass. True strain (ε) was calculated as $-\ln(h_0/h)$, where h_0 and h are the initial and the final thickness of the rolled specimen, respectively. Rolling was performed in non-lubricated conditions using a two-high rolling mill with a roll diameter of 131 mm and a peripheral roll speed of 346 mm/s. Immediately after rolling, the resulting 1.33 mm-thick specimen was water quenched. Afterwards, it was divided in three identical pieces that were supplied to the next ARB pass. From then on, the procedure described above was executed 4 more times maintaining the rolling direction (RD). The schematic illustration of the ARB process carried out in the present investigation is shown in Fig. 1.

The microstructure of the as-received material and the ARBed samples were examined by optical microscopy (OM) and transmission electron microscopy (TEM), respectively. Examinations were made on the rolling plane in a section located at a depth of 40% from the surface. The OM studies were carried out in an Olympus BH-2 microscope equipped with a

Table 1. Chemical composition of the 7075 Al alloy studied (mass%).

Zn	Mg	Cu	Cr	Fe	Si	Ti	Mn	Al
5.68	2.51	1.59	0.19	0.19	0.052	0.025	0.007	bal.

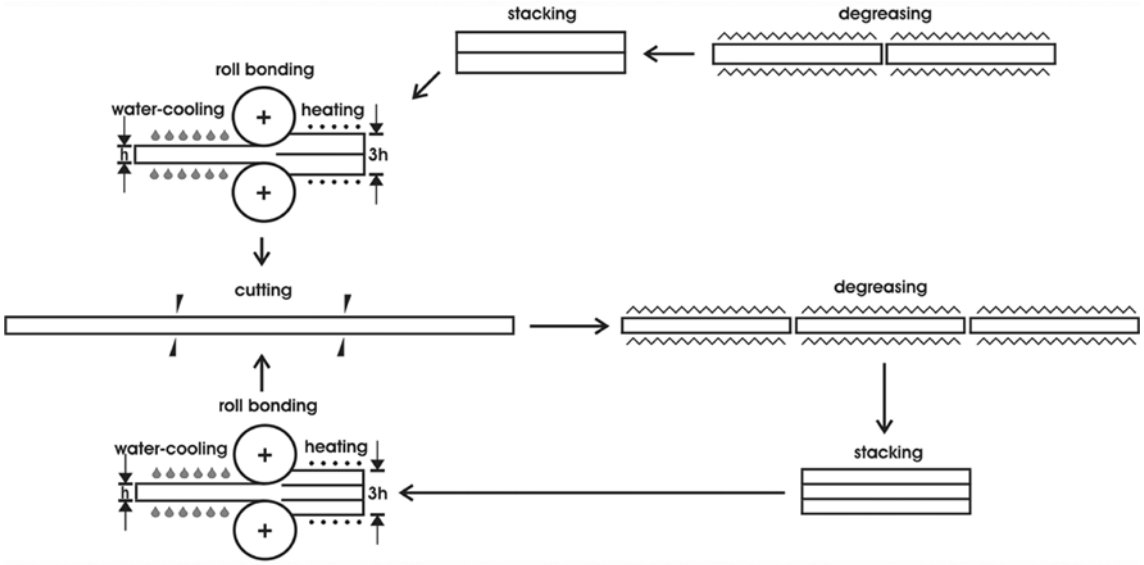

Figure 1. Schematic illustration showing the ARB process carried out in the present investigation.

digital camera, while the TEM studies were carried out in a JEOL JEM 2000 FX II microscope operating at 200 kV. The mean cell/(sub)grain size (d) of the ARBed samples was calculated from TEM micrographs as the mean boundary spacing. The specimens for the OM investigations were etched with Keller's reagent. For the TEM investigations, disks of 3 mm diameter extracted from the ARBed samples were thinned to perforation using a twin-jet electropolishing facility with a solution of 30% nitric acid and 70% methanol at 15 V and -25ºC.

In order to investigate the crystallographic features of the ARBed samples, electron backscatter diffraction (EBSD) measurements were conducted in a JEOL JSM 6500 F field emission gun scanning electron microscope (FEG-SEM) operating at 20 kV with a working distance of 15 mm. The EBSD measurements were performed on the rolling plane in a section located at a depth of 40% from the surface. The data acquisition and analysis were performed using the commercial Channel 5 software. Because of the limited angular resolution of the EBSD system, misorientations below 2º were neglected. The boundaries with misorientations from 2º to 15º were defined as low angle boundaries (LABs), while those with misorientations greater than 15º were defined as high angle boundaries (HABs). From EBSD data, the mean

boundary misorientation angle (θ) of the ARBed samples was quantitatively determined. The specimens for EBSD investigations were electropolished in the same solution that was used for the TEM specimens at 15 V and -15ºC.

Textures were determined by X-ray diffraction in a section located at a depth of 40% from the surface. The (111), (200) and (220) pole figures were measured using CuK_α radiation in a Siemens D500 diffractometer equipped with an open Euler ring working with Schultz geometry. From these experimental pole figures and using the TexTools software, the orientation distribution functions (ODFs) were derived by means of the series expansion method. In this paper, the ODFs are represented in form of sections through the Euler space which, due to the cubic crystal symmetry and the orthorhombic sample symmetry, is defined by $0º \leq \varphi_1, \Phi, \varphi_2 \leq 90º$. In particular, equal distance sections along the φ_2 angle in 5º steps are used. Also, for a better understanding of the texture evolution, the β-fibre was directly measured from the ODFs.

Tensile specimens with a gauge length of 10 mm and width of 3 mm were electro-discharge machined from the as-received sheet and the ARBed samples with their tensile axis perpendicular to RD. Uniaxial tensile tests were performed at 300ºC using a Servosis ME 405/10 testing machine and an elliptical furnace provided with four quartz lamps. The specimens were pulled to failure with a constant rate of crosshead displacement giving an initial strain rate of 10^{-2} s^{-1}. They were held at the testing temperature for 20 min before the tests and water quenched immediately after the tests. The true stress (σ)-true strain (ε) curves were calculated using standard expressions. From the curves, the yield stress ($\sigma_{0.2}$) and the maximum stress (σ_{max}) were estimated as the flow stress at 0.2% strain and as the maximum value of the flow stress, respectively. The elongation to failure (e_F) was also determined. After the tests, the gauge section surface of the tensile specimens was examined in a HITACHI S 4800 cold FEG-SEM.

3. Results

Observations made by optical microscopy (Fig. 2) reveal the presence in the as-received material of relatively equiaxed grains in the rolling plane (Fig. 2(a)), but flattened in the normal direction (ND) (Fig. 2(b)). That is, in contrast to the typical elongated morphologies of the as-rolled material, a microstructure composed of pancake shaped grains of dimensions 60 x 47 x 4 μm^3 is present, which is attributed to the T6 thermal treatment. On the other hand, the complete ODF (Fig. 3) shows that texture of the as-received material is dominated by the cube (C) orientation $(\varphi_1,\Phi,\varphi_2)$ = (0º,0º,0º) and the rotations of this orientation along RD, visible along Φ at φ_1= 0º in the φ_2= 0º/90º-section, with intensities along the entire fibre between the C, at Φ = 0º, and the Goss (G), at Φ = 45º, positions.

TEM micrographs of the ARBed samples are displayed in Fig. 4. The 1-pass sample (Fig. 4(a)) exhibits cells with a high dislocation density inside and dislocation-tangling zones. In the 2-passes sample (Fig. 4(b)) dislocation density is quite low and defined boundaries are seen. However, some of the boundaries are still diffused, resembling a cell structure. In the 3-passes sample (Fig. 4(c)) (sub)grains surrounded by well-defined boundaries with a low dislocation density inside are already clearly seen. Finally, the 4-passes (Fig. 4(d)) and 5-passes (Fig. 4(e)) samples are covered with well-contrasted and equiaxed (sub)grains. In

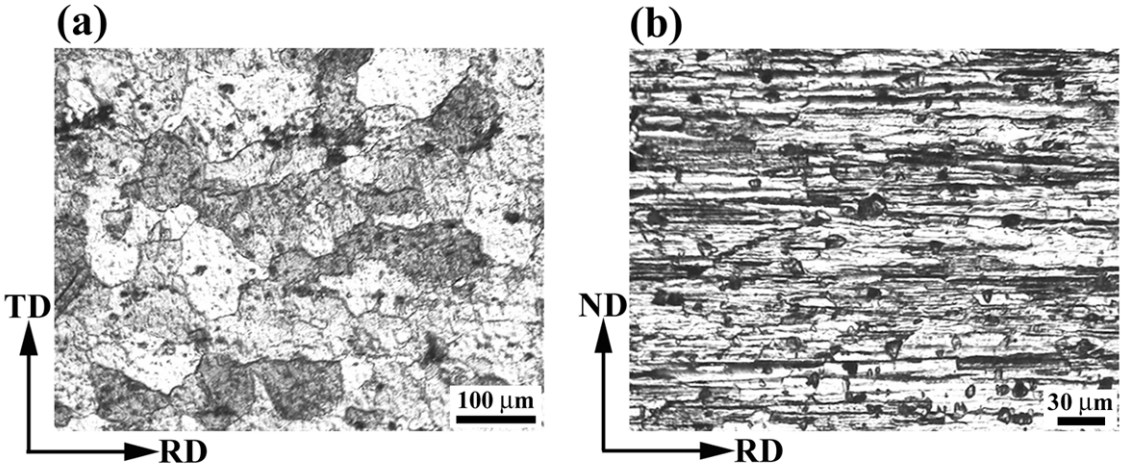

Figure 2. OM micrographs of the as-received material on the (a) rolling and (b) longitudinal-transverse planes.

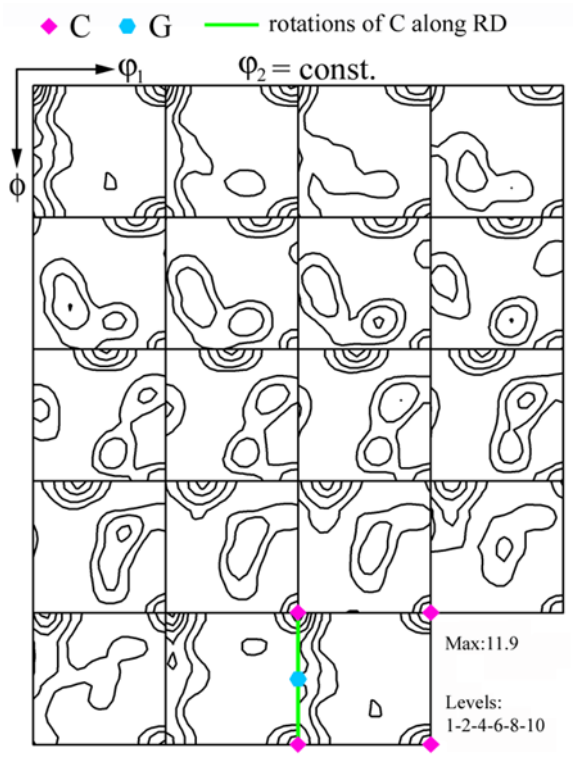

Figure 3. ODF of the as-received material.

summary, the TEM micrographs reveal a gradual evolution from a microstructure with cell walls and elevated dislocation density to a microstructure composed of sharp boundaries with low dislocation density within. It is worth noting that the most significant changes take place during the first three passes. Then, changes are less pronounced. Lastly, the TEM micrographs also show that the mean particle size increases with increasing N.

EBSD maps of the ARBed samples are displayed in Fig. 5. In the grain boundary (GB) maps, LABs are depicted as grey lines, while HABs are depicted as black lines. The colours in the ND and RD maps represent the crystallographic directions parallel to ND and RD, respectively. The correspondence between the colours and the crystallographic directions is indicated in the standard stereographic triangle shown in the picture. Fig. 5(a) exhibits mainly some fragments of grey lines, indicating that the 1-pass sample essentially contains boundaries with misorientations below 2º or cell walls. Moreover, according to Fig. 5(b) and (c) the microstructure of this sample is characterized by large grains with a relatively low

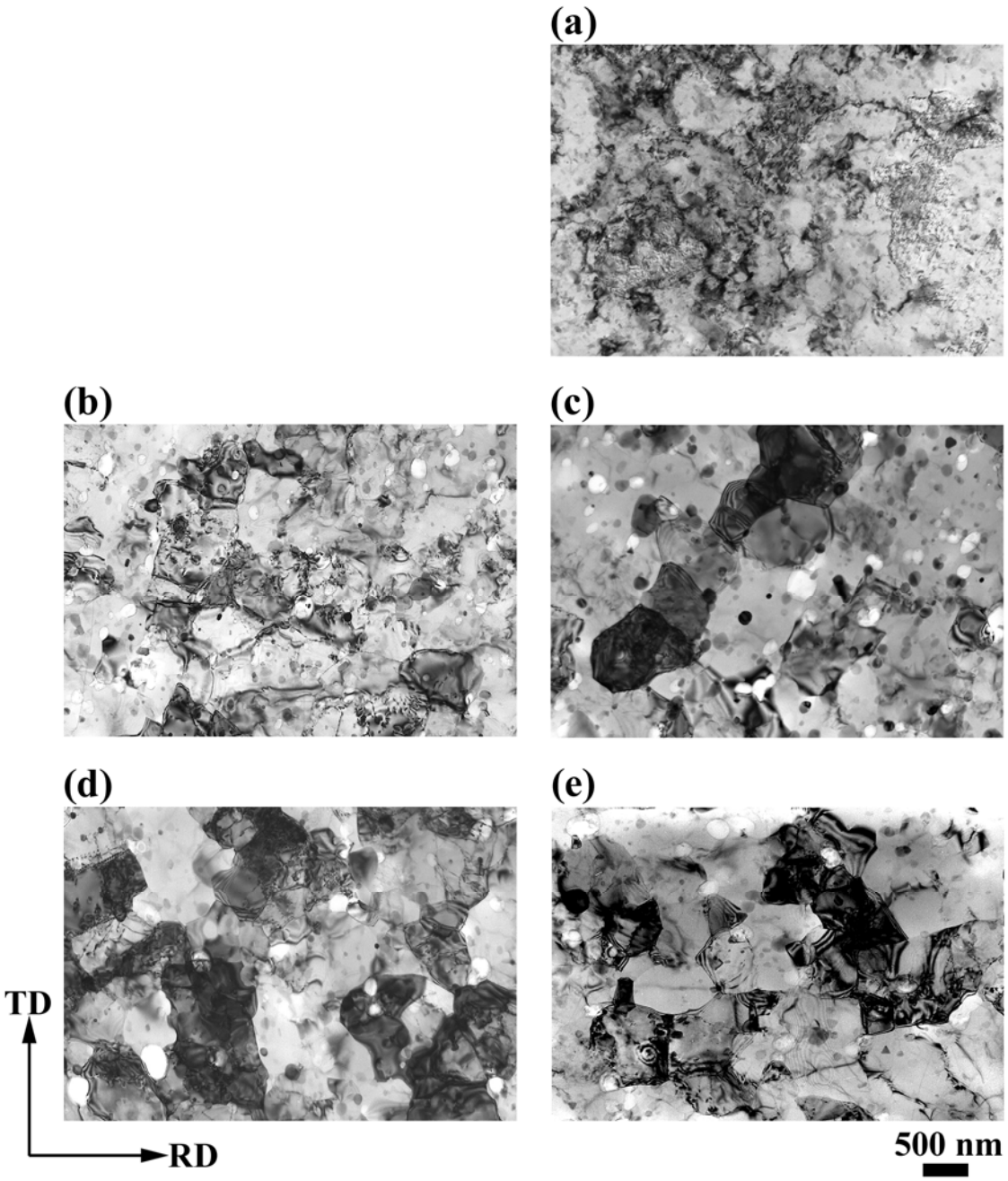

Figure 4. TEM micrographs of the (a) 1-pass, (b) 2-passes, (c) 3-passes, (d) 4-passes and (e) 5-passes samples.

orientation gradient inside. This is consistent with the presence of a cell substructure inside the original grain structure. Fig. 5(d) shows that the 3-passes sample comprises both LABs and HABs, indicating that its microstructure consists of (sub)grains. Additionally, the spatial distribution of the orientations in this sample (Fig. 5(e) and (f)) is much more homogeneous than in the 1-pass sample. This is consistent with a quick transition from a cell structure to a (sub)grain structure during the first three ARB passes. Fig. 5(g) shows that the microstructure